EPJdirect A1, 1–11 (2003)
DOI 10.1007/s1010503a123

EPJdirect
electronic only

Early Physics Reach of CMS

K. Hoepfner on behalf of the CMS collaboration

RWTH Aachen, Sommerfeldstrasse, D-52056 Aachen, Germany
e-mail: kerstin.hoepfner@physik.rwth-aachen.de

Received:

Abstract. When the LHC turns on, CMS will have most of the detector ready, except some (minor) staged items. The commissioning of the detector and the impact of stageing is discussed. The physics potential of the first physics run, anticipated to provide an integrated luminosity of up to $10\,\mathrm{fb}^{-1}$, is demonstrated using examples on Higgs boson and Supersymmetry particle searches.

PACS: CMS, Higgs boson, Supersymmetry, $10\,\mathrm{fb}^{-1}$ physics

1 The CMS Experiment

The Compact Muon Solenoid (CMS) Experiment, one of two multi-purpose experiments being constructed at the future Large Hadron Collider (LHC) at CERN, envisages a rich physics program. The main feature of CMS is its compact design and a superconducting coil providing a four Tesla magnetic field. The tracking system and both calorimeters are placed inside the coil. The muon system is merged with the return yoke for the magnetic field. As a colliding beam experiment, CMS is symmetrically arranged around the interaction point at the centre of the detector (Fig. 1). Nearest to the interaction point is a high-resolution pixel vertex detector, followed by a large silicon strip tracker, an electromagnetic calorimeter made of lead tungstate crystals, a brass-scintillator-tile hadron calorimeter and, a muon system exploiting three different varieties of gaseous detectors (drift tubes in the barrel, cathode strip chambers in the forward regions and resistive plate chambers in both, barrel and endcap regions for triggering purpose). Very forward particles are detected in quartz fibre calorimeters.

To select the interesting physics from the background, which is several orders of magnitude larger in rate, CMS exploits a trigger system with two levels. The first level in the trigger is implemented in hardware. Further triggering is implemented in software in the "Higher Level Trigger" (HLT).

The commissioning and start-up of the experiment is driven by the schedule of the LHC machine. A possible start-up scenario [1], consists of three phases:

Phase 1: LHC commissioning to set up the accelerator. Starting with one, low intensity beam, then two beams and slowly increasing the number of low-itensity bunches. At the startup the luminosity will be around 10^{27} cm^{-2} s^{-1} and is expected to rise to 10^{32} cm^{-2} s^{-1}. The CMS collaboration will study the detector performance, debug data handling, synchronize detectors and catalog detector problems in addition to recording halo-muons and first proton-proton collisions.

CMS wishes to have a shutdown after the LHC commissioning phase to fix potential detector problems and install the vertex detector. The present schedule also allows for an earlier installation which might allow for an early commissioning of the pixel detector which enhances the combined performance of the detector.

Phase 2: First physics run with 25 ns spaced proton-proton collisions. Assuming a scenario with 10 hours filling time, a run of 14 hours (one fill per day), a luminosity lifetime of 20 hours and a moderate data-taking efficiency of 66%, one month of running at $\mathcal{L} = 10^{33}$ cm^{-2} s^{-1} would yield about 0.7 fb^{-1} of statistics. With an anticipated luminosity of 1-2 $\times$ 10^{33} cm^{-2} s^{-1}, 5-10 fb^{-1} may be accumulated over a seven-month running period.

Phase 3: High luminosity running at $\mathcal{L} = 10^{34}$ cm^{-2}s^{-1} is anticipated for the second or third year of operation. The physics accessible is described in [2].

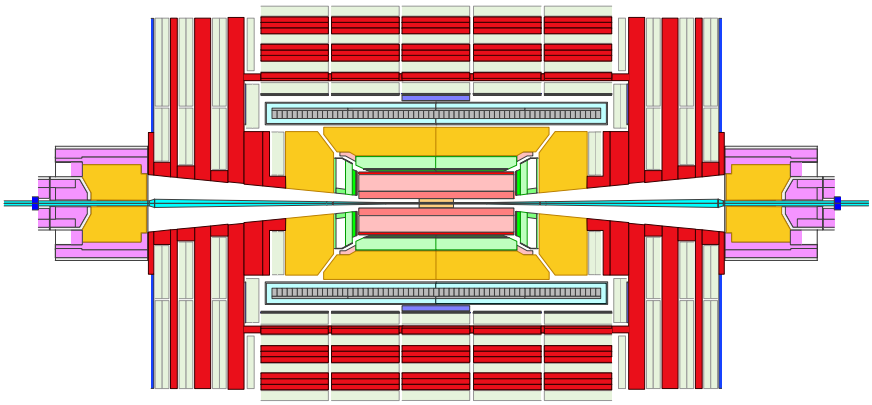

Fig. 1. Transverse view of the CMS Detector with the interaction point at the centre. Interaction products are detected (from the inside out) by a pixel vertex detector, a silicon strip tracker, electromagnetic crystal and hadron tile calorimeters and a muon system. Very forward calorimeters made of quartz fibres are on both ends of the detector.

1.1 The CMS Detector at Start-up

The initial detector will be the complete CMS, as shown in Fig. 1, except for a few items as necessitated by the financial planning of the experiment. Most subsystems, such as the tracker, the electromagnetic and hadron calorimeters, and the muon barrel system will be complete at this stage. The components that will be staged are:

- Half of the data aquisition (DAQ) which results in the largest saving. The Event Builder of the CMS DAQ consists of eight units each one capable of transporting 12.5 kHz of events, for a full design capability of 100 kHz.

The reduced luminosities expected during the first year of LHC operation lead to fewer pile-up events and correspondingly reduced data volumes per event. About two pile-up events are expected as compared to about twenty at high luminosity. At start-up four out of eight DAQ slices are foreseen, leading to a rate capability of 50 kHz. The reduced DAQ requires careful tuning of the trigger thresholds throughout the multi-level trigger chain in order to preserve the interesting physics.

- The pixel detector will be complete except for the outermost endcap station. The stageing of the third endcap layer will cause a small loss in efficiency and redundancy. The loss is acceptable, since most tracks going through the endcaps also hit at least one barrel layer as well.
- In the muon endcap system the outermost tracking station is completely staged. The cathode strip chambers for tracking and the resistive plate chambers for triggering will not be available during initial low-luminosity running. Consequences are discussed in the following.
- In addition, of the remaining three muon endcap stations, resistive plate chambers will only be available up to a pseudorapidity $|\eta| > 1.6$, amounting in total to 1/3 of the RPC system. The full geometric acceptance is provided by the CSC system, which is instrumented up to $|\eta| = 2.4$.

The physics requirements that lead to the above staging scenarios are:

- Maximal geometrical acceptance for electrons, muons and jets.
- Complete and hermetic hadron calorimeter system to guarantee a good measurement of missing energy $E_T^{\rm miss}$.

1.2 Trigger Rates

The level-1 trigger uses fast information from the muon and calorimeter systems only. Its task is to reduce the 40 MHz crossing rate to 50 kHz of interesting physics events, the maximum bandwidth of the DAQ system at the beginning. Table 1 summarizes the Level-1 trigger rates. The rates per data stream are defined by requiring equal sharing for the four classes "e/γ", "muon", "tau" and "jet". With an additional factor three for safety, only 16 kHz are allocated in total.

The rest of the online selection is performed by the High-Level Trigger (HLT) running on a powerful farm of commercial processors (1000 dual processors at the beginning). The HLT selection is carried out in successive virtual "trigger levels":

"Level-2" exploits the full calorimeter and muon information

"Level-2.5" uses only the pixel information

"Level-3" refers to the use of the full tracker information

Table 2 shows the thresholds, rates and event mixture achieved by the HLT for an output rate to permanent storage of about 100 Hz at a luminosity of $2 \times 10^{33}{\rm cm}^{-2}{\rm s}^{-1}$ [4].

Channel	Threshold [GeV] $\epsilon = 0.95$	Individual Rate [kHz]
Inclusive isolated e/γ	29	3.3
Dielectrons/Diphotons	17	1.3
Inclusive isolated muon	14	2.7
Dimuons	3	0.9
Single tau jet trigger	86	2.2
Two tau jets	59	1.0
One, three or four jets	177, 86, 70	3.0
Jet $\times$ $E_T^{\rm miss}$	88 $\times$ 46	2.3
Electron $\times$ jet	21 $\times$ 45	0.8
Min-bias (Calibration)		0.9
Total allocated rate		16

Table 1. Expected first level trigger rates at low luminosity [3] The thresholds quoted correspond to the values in momentum/energy for which the trigger is 95% efficient. The sum of the rates is larger than 16 kHz due to overlap between the channels.

2 Commissioning of the Detector

Interesting physics can be done right from the start-up of LHC provided the trigger functions efficiently. To reach this goal, a minimal calibration and detector mastering is necessary, which is discussed in the following. In brief, the level-1 and level-2 triggers require that the muon system is aligned to about 1 mm and that the calibration of ECAL and HCAL are known to about 2% (see Sections 2.2 and 2.3). The level-2.5 trigger requires a functioning pixel system properly aligned to $\sim$10 μm while the level-3 trigger relies on a a functioning silicon strip tracker aligned to $\sim$20 μm (see Section 2.4).

Channel	Threshold [GeV] $\epsilon = 0.9...0.95$	Rate [Hz]
One or two electrons	29 , 17 + 17	34
One or two photons	80 , 40 + 25	9
Single muon, Dimuon	19 , 7 + 7	29
Single tau jet, Two jau jets	86 , 59 + 59	4
One, three or four jets	657 , 247 , 113	9
Jet $\times$ $E_T^{\rm miss}$	180 + 123	5
Electron $\times$ jet	19 + 45	2
Inclusive b jets	237	5
Calibration, other		$\sim$10
Sum		105

Table 2. Expected high-Level trigger rates at low luminosity [3].

2.1 Aspects of Muon System Commissioning

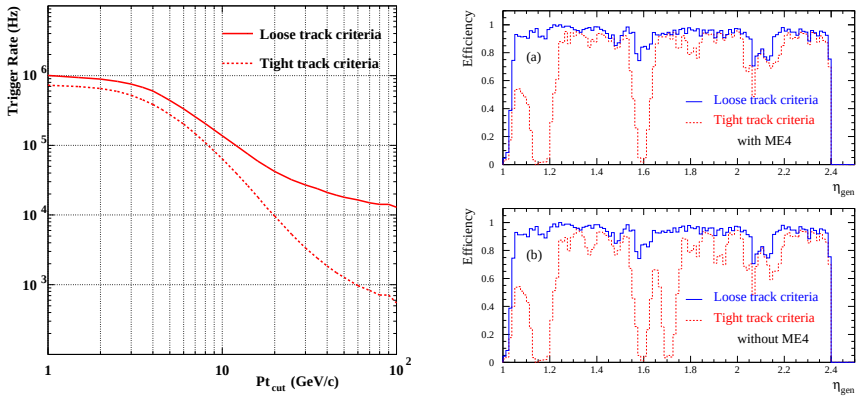

(a) Trigger rate. (b) Efficieny.

Fig. 2. Trigger rate and efficiency of the CSC system with and without the outermost muon endcap station (ME4). "Tight" tracking criteria (meaning three hits out of three stations) lead to a moderate trigger rate but shows deep holes in the efficiency [6].

Muon identification is provided by absorption of all other particles (except neutrinos) in the preceeding calorimeters and magnet coil and tracking in four muon stations inserted in the iron return yoke of the magnet.

The CMS muon trigger system is characterized by high redundancy. Both barrel and endcap systems feature two complementary trigger information - drift tubes (DT) and resistive plate chambers (RPC) in the barrel; cathode strip chambers (CSC) and RPCs in the endcap. The level-1 and level-2 muon triggers rely on standalone muon measurements. An accurate p_T measurement is obtained by measuring the bending angle of the muon at the exit of the four Tesla magnet, assuming the muon originates at the beam spot.

A precision $\Delta p_T/p_T$ ~10% is achieved for all transverse momenta up to 200 GeV/c. The measurement is dominated by multiple scattering in the material before the first muon station (calorimeter and magnet). The requirement on the first muon station position is ~1 mm. The level-3 muon trigger relies on a matching of the muon track with the inner tracker measurement and drastically improves the p_T resolution to ~1%. This requires that the inner tracking system is internally aligned to ~20 μm. The matching procedure requires the position of the muon system with respect to the tracker to be known to about 1 mm.

The outermost endcap station (CSC and RPC) and RPC chambers covering the region $|\eta| > 1.6$, have been staged. Studies of the impact of the staged items at high η show that, without RPC and CSC in coincidence in the general muon trigger, some valuable redundancy is lost. Indeed with two out of three stations (the so-called "loose" tracking criteria in Fig. 2), the p_T resolution is

not sufficient for level-1 rate reduction leading to an order of magnitude higher trigger rate in this region for $p_T \geq 20$ GeV/c [6].

Very "tight" tracking criteria succeed in keeping the trigger rate at a moderate level (Fig. 2a) but generate holes in the efficiency distribution (Fig. 2b). This is particularly pronounced in the region $|\eta|$ >1.6, where the RPCs are not available to resolve the CSC ambiguities which are naturally present by construction (crossed wires and cathode strips).

The two options to keep high efficiency are

1. Trigger demanding only two out of any three chambers in the region $1.6 < |\eta| < 2.1$. This results in a trigger rate which is higher by a factor ten.

2. Restore the inner part of the fourth endcap muon station (ME4/1) to have information in the region with no RPC chambers. This option is presently under consideration.

At start-up, the performance of the individual detectors will have been assessed from production tests with cosmics and testbeams. Less known are the positions of the various substructures with respect to each other. The alignment system will give the positions of the five mechanically independent barrel wheels and the two endcaps with sub-millimetre precision. A subsequent alignment using reconstructed tracks from beam-halo muons and also from $W \rightarrow \mu\nu$ and $Z \rightarrow \mu\mu$ events leads to the desired precision, in particular in the $r\phi$ bending plane which is critical for the measurement of the muon p_T.

2.2 The Electromagnetic Calorimeter

The CMS electromagnetic calorimeter [7] consists of 75848 lead tungstate crystals and covers pseudorapidities up to $|\eta| = 3.0$. Light created in a crystal by electromagnetic showers is read out with avalanche photodiodes (APD) in the barrel region and photo-triodes in the endcaps. Subsequently, the signal is amplified and filtered in the front-end electronics.

The HLT selection of e/γ requires:

1. The electromagnetic calorimeter to be calibrated to ~2%.

2. A working pixel system.

Identification of electrons and photons in the HLT is obtained by first combining clusters reconstructed in the ECAL into "superclusters" for a better estimate of the e/γ E_T (than is available at Level-1). The next step uses fast matching of ECAL clusters to tracks in the pixel system. This requires a fast mastering of the alignment of the three barrel layers and the two endcap disks of the pixel system. The commissioning of the tracker is discussed in Section 2.4.

The benchmark channel for the ECAL $H \rightarrow \gamma\gamma$ requires the best possible energy resolution. The ultimate resolution of 0.5% will eventually be achieved offline, by intercalibrating each individual crystal with large samples of electrons

from W decays. At start-up however, the ultimate resolution is not needed. As previously mentioned only a ∼2% calibration is required very fast for the trigger.

A fast method [8] based on minimum-bias crossings will be applied. In addition, measurements obtained during module production and test beam calibrations will be exploited.

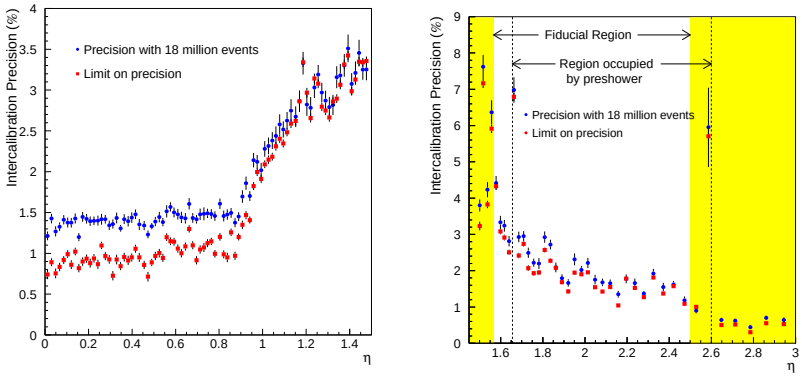

(a) Barrel. (b) Endcaps.

Fig. 3. ECAL intercalibration precision obtainable with 18 million minimum-bias events in comparison to the precision limit for very large statistics [8].

1. **During production:** A raw intercalibration precision is obtained during production from laboratory measurements with a radioactive source. The crystal light yield and the response of APD and front-end electronics are determined. Measurements on about 90 crystals have shown an intercalibration precision of ∼4.5% [9]. This information is stored in the database and related to a measurement of a few modules in the testbeam.

2. **Testbeam:** A few modules will be calibrated in the testbeam. In the final detector these modules will be uniformely distributed to act as "standard candles". The transfer of the testbeam calibration, after module transport, installation, etc., is expected to be ∼2%. The present construction and testbeam schedule implies that about 25% of all ECAL modules can be pre-calibrated.

3. **Rapid intercalibration using minimum bias events:** At the beginning, the entire detector will not be functioning optimally, a pre-requisite for a calibration procedure using electrons from Z or W events. A rapid intercalibration method [8] exploits the uniformity of energy deposition in minimum-bias events to intercalibrate pairs of rings of crystals at fixed pseudorapidity. The number of intercalibration constants is reduced from 75848 (number of crystals) to 125 (number of ring pairs of fixed pseudorapidity).

The precision is limited by inhomogenities at fixed η which break the ϕ symmetry and by the total radiation length thickness of the tracker which varies from 0.5 X_0 to 1.2 X_0 as a function of the pseudorapidity η.

A sample of 18 million minimum-bias events provides a precision between 1.2% and 4.5% (Fig. 3) throughout the fiducial region, comparable to the ultimate accuracy reachable with very large statistics. With a level-1 bandwidth of 1 kHz, these 18 million events can be recorded within three hours, which is included in the current trigger tables.

The intercalibration in η of the 125 rings of crystals can be performed rapidly using electrons from Z decay and checked against the "candle" supermodules previously calibrated in the test beam.

Once the tracker is fully operational the final goal of $\Delta E/E = 0.5\%$ for $H \to \gamma\gamma$ will be reached off-line by calibrating individual crystals with real electrons from W decays (see [9]).

2.3 The Hadron Calorimeter

The CMS hadron calorimeter [10] is a brass-scintillator tile calorimeter with a barrel and two endcaps located inside the magnetic field, covering pseurorapidities up to $|\eta|$=3. Two very forward calorimeters surrounding the beam pipe extend the coverage up to $|\eta|$=5.

Its primary physics task is the measurement of jets, with energy up to 3 TeV, and of missing energy. The latter requires a good hermeticity. As seen in Table 2 several trigger channels rely on E_T^{miss}, tau and jet selection using HCAL information.

While the HCAL has a moderate jet transverse energy resolution ($\Delta E_T/E_T \sim$ 10% at $E_T \sim$100 GeV) its calibration needs to be known to about 2% for the trigger to function.

The detector itself is essentially already finished and commissioning is ongoing, with testbeam and radioactive source calibration data. A variety of tools is exploited to calibrate the detector and monitor the response while operating. During production the respone of every tile which includes scintillator, the coupling to a wavelength shifting fibre, the response of the hybrid photodiode detector and the readout electronics chain is determined with about 10% accuracy. The main calibration tool is a moving radioactive source, which can illuminate every scintillator tile before the installation of the HCAL.

The response to electrons, muons and pions in the testbeam along with the data taken with the radioactive source demonstrate that the HCAL towers can be calibrated with the source to ~2% without exposure to the beam.

A detailed study of the pulse time structure has also been performed with testbeam data. A unique bunch crossing identification is essential and only possible if the signal is not too spread out. The measurements show that 76% of the signal can be contained the first bunch. The remaining 24% of the signal is seen in the subsequent bunch crossing, which is an acceptable fraction even at high luminosity given the moderate occupancy of the HCAL towers.

The calorimeter response has to be monitored and the calibration to be maintained at 2%. The tile response and transparency change with irradiation are monitored with LEDs, lasers and radioactive sources. During a shutdown, when the CMS detector is opened and the magnetic field is switched off, the radioactive source can again illuminate every individual tile and repeat the above mentioned calibration procedure.

Most important for the CMS physics program are the dijet mass resolution and the jet response. Back-to-back γ + jet events will be used to determine jet energy correction factors as a function of E_T^{jet}.

2.4 Inner Tracking and Alignment

The factor ∼1000 reduction in rate achieved by the High-Level Trigger is obtained by using the inner tracker information. The e/γ selection and the τ selection rely on a working pixel system [4]. The single-muon and dimuon rates above the thresholds given in Table 2 require a precise (∼1%) momentum reconstruction in the silicon tracker. To apply isolation cuts, especially for the tau trigger, it is essential to reconstruct low-momentum particles in the tracker.

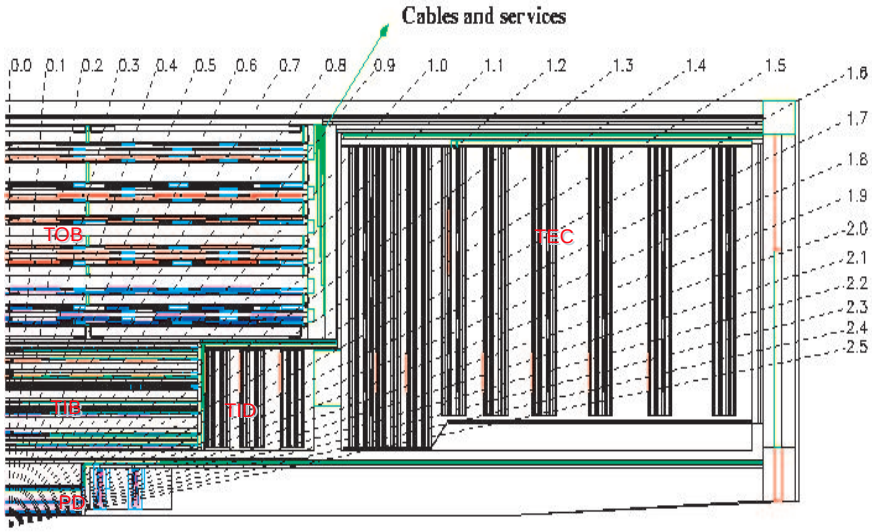

Fig. 4. One quarter of the CMS tracker. Close to the interaction point are high-resolution pixel layers, surrounded by the inner barrel, outer barrel and two endcaps of the silicon strip tracker.

The inner tracking system [12], as depicted in Fig. 4, consists of a pixel detector (∼40 Million channels) followed by a silicon strip tracker (10 Million channels). The latter is composed of four mechanically independent structures: the inner barrel, the outer barrel and two endcaps. Silicon detectors close to the interaction region and near boundaries between the subcomponents are double-sided for reasons of redundancy and detection efficiency. The pixel detector consists of three barrel layers and two endcap disks on each side.

The silicon strip and pixel detectors are positioned with a precision given by that of the support structure and will be surveyed before installation.

The first task after the installation of the tracker will be to align all its components in a single reference frame. The alignment procedure should aim at matching the intrinsic precision of the pixel and silicon strip detectors (10-20 μm). The final alignment with an accuracy of $\sim$10 μm in all three dimensions will be achieved using algorithms based on tracking data obtained with the first minimum-bias collisions. The survey data provide the starting points in these algorithms.

The relative alignment of the tracker and muon systems is not guaranteed during detector operation. Changes in temperature (e.g. when opening the tracker), movements of the muon chambers due to the turning on and off of the magnetic field and due to gravity are expected. To cope with these movements, the detector positions are monitored by a dedicated alignment system, realized by hardware components. The system is complemented by alignment using reconstructed charged particles tracks. Detector positions should eventually be monitored with a precision of 10 μm for the silicon tracker and 100 μm for the muon system.

The alignment system including muon and tracker components and the link between them, is depicted in Fig. 5 The difficulties are *(i)* the long lever arm of about seven meters per side and, *(ii)* a $\Delta T = 40$ K between the ambient temperature in the muon system and the -20°C in the tracker.

At the LHC start-up, the relative alignment of the muon system with respect to the tracker needs to be known to only a few mm for the trigger. The ultimate momentum resolution for very high p_T muons ($p_T > 200$ GeV/c) will be reached offline after alignment of the muon system with respect to the tracker to $\sim$100 μm.

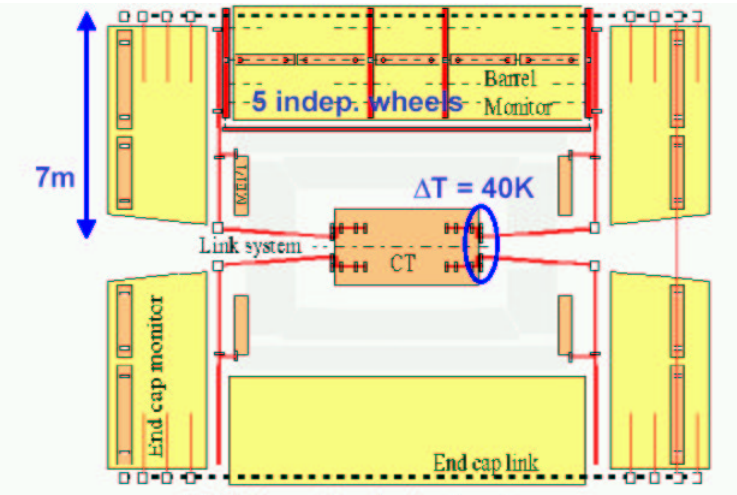

Fig. 5. A dedicated alignment system will monitor the positions of muon chambers (thin lines), relate the muon barrel with the muon endcap (dashed line), and muon system with the tracker (thick solid lines).

3 Early Physics

At start-up of the LHC, a low luminosity of $\mathcal{L} = 10^{33}$ cm^{-2} s^{-1} is expected, as described in Section 1. The trigger thresholds from Table 2 are anticipated to result in the rates given in the same table.

A large fraction of the data stream comes from muon, electron and photon candidates. The muons and electrons come primarily from W leptonic decays at a rate of 20 Hz for a luminosity of $\mathcal{L} = 10^{33}$cm^{-2}s^{-1}. Almost 100 million $W \to \mu\nu$ events are therefore produced for 10 fb^{-1}. Half of these events are in the CMS acceptance with $|\eta| < 2.1$. Events with a Z boson decaying to two charged leptons occur at a far smaller rate (3 Hz). W and Z events are used for detector calibration (ECAL in particular), studies of well-understood physics as tests of QCD, and also determination of QCD backgrounds.

At $\mathcal{L} = 10^{33}$ cm^{-2} s^{-1} the production of $t\bar{t}$ pairs occurs at a rate of $\sim$1 Hz ($\sigma_{tt} \sim 1$ nb). While such events constitute a background source to searches for Supersymmetric particles, they also offer interesting physics opportunities, such as measurements of QCD processes, top quark properties (mass, spin and couplings) and limits on exotic top decay modes e.g. via neutral currents.

The impact of staging various detector items on the physics program at low luminosity was studied in detail. The following features and detector performance were found to be essential to maintain the major physics potential of the experiment with up to 10 fb^{-1}:

- Lepton identification (electron, muon, tau) specifically for an intermediate Higgs boson mass between 130 and 400 GeV/c^2 into four leptons as $H \to ZZ, WW \to \ell^{\pm}\ell^{\mp}, \ell^+\ell^-\nu_\ell\bar{\nu}_\ell$, but also for many other decay chains with leptons in the final state ($t\bar{t}$, Wtb, WZ, ZZ, $\tilde{q}/\tilde{g}$ etc).

- The ultimate tracking resolution, especially at high momentum, requires a full mastery of the alignment and may take some time. Most Higgs boson and Supersymmetric decay channels, however, can be addressed before the ultimate performance is achieved, by means of tight isolation criteria applied to the reconstructed tracks associated to the leptons (e, μ and τ). What is essential is the ability to efficiently reconstruct tracks with low transverse momentum, down to $p_T \sim 1...5$ GeV/c as well as inside jets.

- To cover the low end of the Higgs boson mass range, the detector will have to be understood as well and as fast as possible. The decay of the Higgs boson into two photons, requires a good energy calibration of the electromagnetic calorimeter and efficient event selection because of the small significance (see Fig. 6), in particular at low luminosity. Achieving the ultimate energy calibration is anticipated to take some time.

- Full calorimetric coverage for jet counting, jet vetoing, and tagging of forward jets. The latter two, for instance, are important for finding the signal and suppressing background in the vector boson fusion channel $qq \to qqH$ followed by the decay $H \to WW \to \ell\nu\ell\nu$. For this channel, as well as for squarks and gluino searches in jets (+leptons) + $E_T^{\rm miss}$ final states, full calorimetry coverage is essential to detect the missing energy that has

been carried away by either neutrinos or neutralinos. Searches for Supersymmetry in previously inaccessible regions of parameter space can start very early.

- A good dijet mass resolution is necessary to search for the lighter scalar Higgs boson from Supersymmetry, which can appear early in squark and gluino decay chains leading to leptons + jets + E_T^{miss} as a final state. Top-quark reconstruction demands a good dijet separation, and eventually provides also a way for measuring the dijet mass resolution directly from the data.
- Efficient b tagging is required at an early stage of data taking, for $t\bar{t}$ events, $Hb\bar{b}$ associated production in Supersymmetry, and in squarks and gluino cascades leading to $b\bar{b}$. Good understanding of the pixel detector will be vital.

3.1 Standard Model Higgs Boson Search

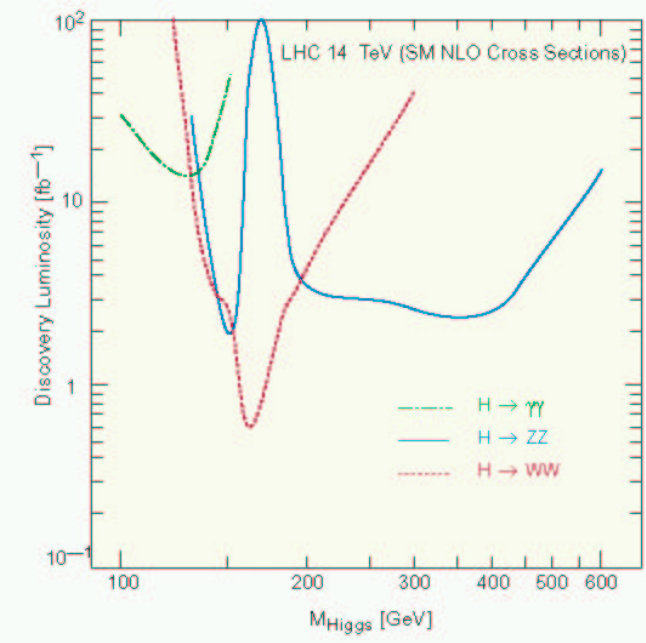

Fig. 6. Discovery luminosity for different channels of the Higgs boson decay.

During the first physics run a data set corresponding to 5 to 10 fb^{-1} may be recorded. The most burning question surely revolves around the search for the Higgs boson. Between now and the LHC start-up the Higgs boson will be searched for by the experiments at the Tevatron. The latter are expected to increase the current limit of 114 $\mathrm{GeV/c^2}$ from LEP. In the best case, they may even provide first evidence for a low-mass Higgs boson. The LHC, and in particular CMS and ATLAS, have been designed to cover the entire Higgs boson mass

range between 80 GeV/c^2 and the theoretical upper limit of 1 TeV/c^2. The first physics run will provide statistics for discovery in channels with large branching ratios and/or a good signal-to-noise ratio. Taking into account the production cross section, the decay branching ratios and the expected signal-to-noise ratio for various selection criteria, the Higgs boson decay modes relevant to the discovery depend on the Higgs boson mass. Fig. 6 shows the expected discovery luminosity for benchmark channels [13].

As can be seen in Fig. 6, the Higgs boson decay into four charged leptons allows a broad mass range to be covered, from $\sim$ 130 to about 750 GeV/c^2 with less than 10 fb^{-1}, however, there is a gap around the WW threshold. With four leptons in the final state an excellent signal-to-noise ratio ($\sim$5:1 depending upon the Higgs boson mass) is achievable in the individual muon or electron and the combined channels. The four-lepton channels demand high efficiencies for charged-particle track reconstruction and for electron and muon identification right from the beginning. A clean signal can be expected in the four lepton channel, assuming successful commissioning of the muon system and the mastery of the alignment. In particular, the muon system will be required to (i) cover the complete acceptance; and (ii) provide a muon reconstruction and identification efficiency in excess of 90%.

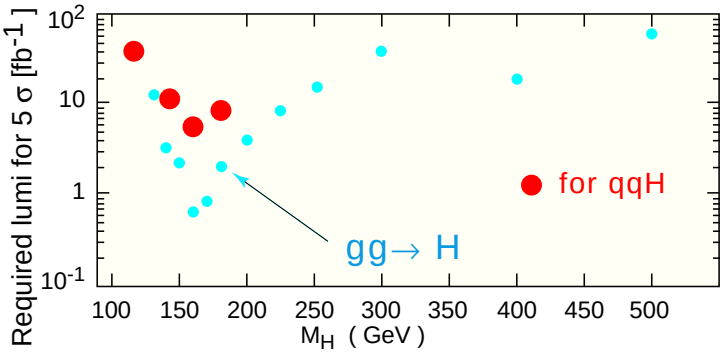

Fig. 7. Required luminosity for a Higgs boson discovery in the gg-fusion and the qqH-channel.

To cover the gap around the WW threshold caused by the drop of the H $\rightarrow$ ZZ branching fraction in this region, the decay H $\rightarrow$ WW $\rightarrow$ $\ell\nu\ell\nu$ needs to be investigated in the two main production modes, the gluon gluon fusion gg $\rightarrow$ H and the vector-boson fusion qq $\rightarrow$ qqH. In both cases, the signature is a pair of charged leptons and a large missing transverse energy $E_T^{\rm miss}$ caused by the two escaping neutrinos. To reject events with fake missing energy, the hadron calorimeter is required to have its full rapidity coverage and hermeticity, as well as a calibration at the percent level.

When produced through gluon fusion, the backgrounds from the Wtb and $t\bar{t}$ processes with leptonic decays of the Ws can be identified and rejected by the tagging of the two energetic and central b jets. This b tagging requires an adequate alignment of the central tracker with an accuracy of 10 microns. The

WW production can be reduced by exploiting the spin correlation of the two Ws in the signal, which leads to a specific distribution of the dilepton openning angle phi, sharply peaked at $\cos\phi = 1$.

In the WW and ZZ fusion processes, two high-energy jets are produced in the very-forward region, and are tagged in the very-forward quartz fibre calorimeter to reject the various background sources. Despite the cross section about 30 times smaller than that of the gluon fusion, this additional handle on the background rejection allows a similar significance to be reached.

Fig. 7 displays the significance for these channels. Already with only a few fb^{-1} of data, a search can begin in the favorite Higgs boson mass bin around 160 GeV.

Finally, small Higgs boson masses need the contribution of the $\mathrm{H} \to \gamma\gamma$ and $\mathrm{H} \to \mathrm{b\bar{b}}$ decay channels, in addition to all of the above. Indeed, the statistics accumulated with an integrated luminosity of $10\,\mathrm{fb}^{-1}$ are too small for a single channel and a single experiment to lead to an unambiguous discovery. Studies for other channels, like associated Higgs boson production, are under way. Using the combined statistics of ATLAS and CMS a significance of around 3-5 becomes possible. Clearly, this channel relies on excellent ECAL calibration.

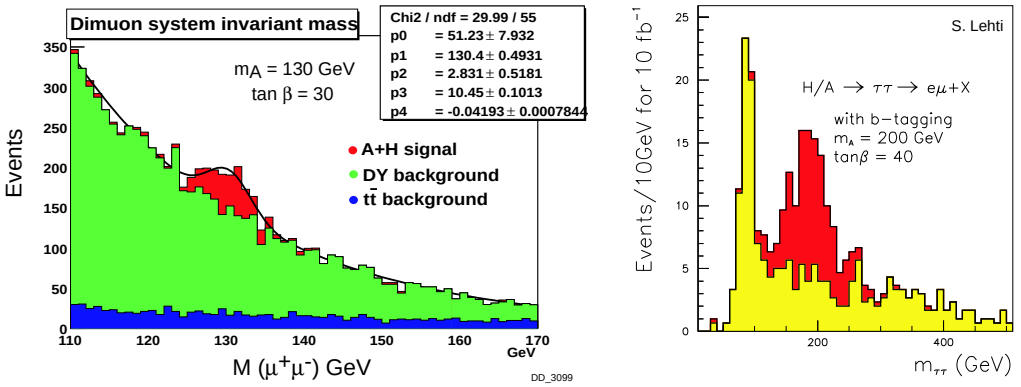

(a) $H/A \to \mu\mu$ (b) $H/A \to \tau\tau$

Fig. 8. MSSM Higgs boson signal: (a) Signal and background in the dimuon spectrum for an integrated luminosity of $20\,\mathrm{fb}^{-1}$, $m_A = 130$ GeV and $\tan\beta = 30$. (b) Electron-muon mass distribution for the decay in $\tau^+\tau^-$ together with the excpected background for an integrated luminosity of $10\,\mathrm{fb}^{-1}$, $m_A = 200$ GeV and $\tan\beta = 40$. [14].

3.2 MSSM Higgs Boson Search

In the MSSM, two Higgs doublets are required and give rise to five physical states, two scalar neutral Higgs bosons, h and H, one pseudoscalar neutral state, A, and two charged Higgs bosons H^+ and H^-. The production and decays of

the lighter scalar h are comparable to that of the standard model Higgs boson, but the associatedcross section for production via the process $gg \to b\bar{b}H/A$ is enhanced by a factor $\tan^2\beta$. Here, $\tan\beta$ is the ratio of the vacuum expectation values of the two Higgs doublets.

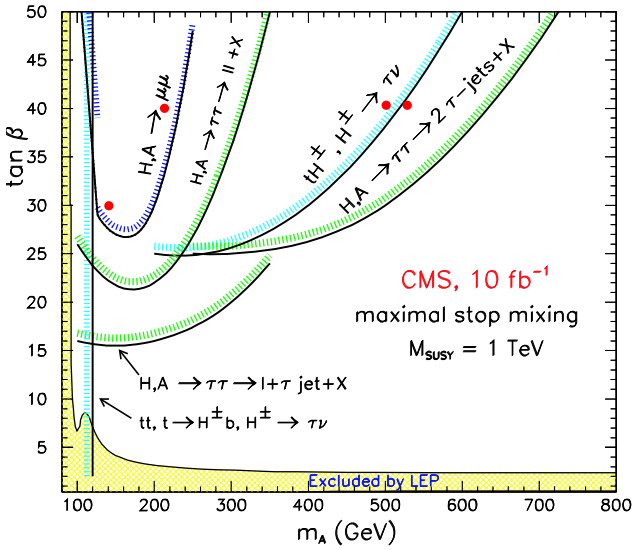

Fig. 9. Regions for MSSM Higgs boson in the $m_A, \tan\beta$ plane which can be accessed with an integrated luminosity of $10\,\mathrm{fb}^{-1}$.

If $\tan\beta$ is large enough, and provided that the b-tagging capabilities are adequate with an appropriate alignment of the tracker, this production process can lead to a discovery with the first few fb^{-1}. The Higgs boson decay channels $H \to \mu\mu$ and $H \to \tau\tau$ were studied in this framework, with a full simulation and reconstruction of the event in the CMS detector. Fig. 8 shows the $\mu\mu$ and $\tau\tau$ mass distributions for $m_A = 130$ and 200 $\mathrm{GeV/c^2}$ and $\tan\beta = 30$ and 40, respectively, with an integrated luminosity of $20\,\mathrm{fb}^{-1}$ and $10\,\mathrm{fb}^{-1}$ respectively. In the muon channel, the signal can be extracted from a large Drell-Yan background thanks to the distinctive signature and good mass resolution.

In the decay channel, $A/H \to \tau\tau$, with either leptonic or hadronic tau decays, a good signal-to-noise ratio can be achieved with $10\,\mathrm{fb}^{-1}$ of integrated luminosity. With good lepton identification and handling of the backgrounds from Drell-Yan, $\gamma, t\bar{t}$, and Wtb, the signal displayed Fig. 8b can be achieved [14].

A significant part of the $(m_A, \tan\beta)$ plane, can be covered with $10\,\mathrm{fb}^{-1}$, as displayed in Fig. 9. With increasing statistics the sensitivity improves rapidly, mainly extending to larger Higgs boson masses.

3.3 SUSY Signatures

The search for supersymmetric particles constitutes another field of study at the LHC which can start at low luminosity. If squarks and gluinos are light enough (below 1 to 2 $\mathrm{TeV/c^2}$), their production dominates the total cross section for the direct production of supersymmetric particles at hadron colliders.

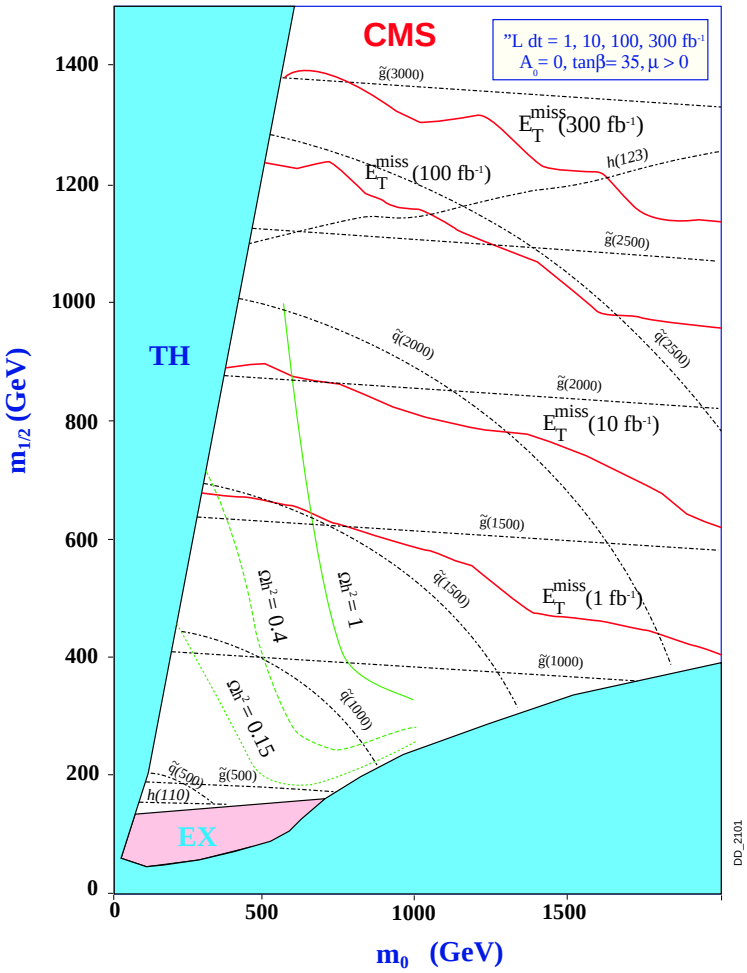

Fig. 10. Reach for inclusive states containing jets and missing energy for various integrated luminosities ($\tan\beta = 35$). Theoretically excluded regions are shaded. The area currently excluded by LEP, reaching to about $m_{1/2} = 100$ GeV, is labelled 'EX'. This limit is expected to be extended by the Tevatron experiments to gluino masses of ~500 GeV. This Tevatron limit can be extended by an order of magnitude with $1\,\mathrm{fb}^{-1}$ of LHC data (roughly one month at 10^{33}).

This large cross section should allow the search for Supersymmetry to lead to a discovery with the first fb^{-1}. Because squarks and gluinos decay in turn to lighter SUSY particles, the final states are in general characterized by many jets, leptons and large missing transverse energy. The potential of this search is exemplified in Fig. 10 in the (m_0, $m_{1/2}$) plane of the mSugra model, a very constrained version of the MSSM. Gluino and squark masses up to 1.5 $\mathrm{TeV/c^2}$ are accessible with about $1\,\mathrm{fb}^{-1}$. This requires efficient lepton identification and complete calorimeter coverage immediately after the LHC start.

3.4 Reconstruction of Supersymmetric Particles

The observation of an excess of events over the Standard Model expectation is not sufficient to find out which SUSY scenario is at work. Rather, if new particles are involved, it is necessary to measure their masses and couplings to Standard Model particles. The CMS capability to reconstruct squarks and gluinos was investigated within mSugra, in the very favourable so-called point B [16], for which gluinos, squarks and in particular sbottoms are light and copiously produced. The following decay chains were examined.

a) $\tilde{g} \to \tilde{b}\bar{b} \to \chi_2^0 b\bar{b} \to \tilde{\ell}^{\pm}\ell^{\mp} b\bar{b} \to \chi_1^0 l^{\pm}\ell^{\mp} b\bar{b}$

b) $\tilde{g} \to \tilde{q}\bar{q} \to \chi_2^0 q\bar{q} \to \tilde{\ell}^{\pm}\ell^{\mp} q\bar{q} \to \chi_1^0 \ell^{\pm}\ell^{\mp} q\bar{q}$

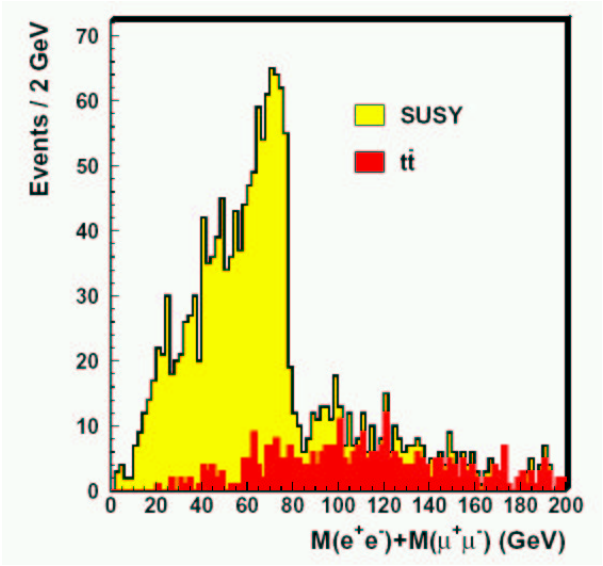

Fig. 11. Invariant mass of oppositely-charged same-flavour lepton-pairs with $E_T^{\mathrm{miss}} > 150$ GeV and $E_{\ell\ell} > 100$ GeV superimposed on the Standard Model background [15].

For both decay chains, the χ_2^0 is identified by a pair of oppositely-charged same-flavour leptons from the decay $\chi_2^0 \to \tilde{\ell}^{\pm}\ell^{\mp} \to \ell^+\ell^-\chi_1^0$. If the mass of

the lightest neutralino is known (from other measurements or from a fit to the dilepton kinematics) and assuming (within mSUGRA) that $m_{\chi_2^0} \sim m_{\chi_1^0}$, the mass and the momentum of the χ_2^0 can be reconstructed from the edge of the dilepton invariant mass distribution (Fig. 11): this end point corresponds to the specific kinematic configuration in which the leptons are back to back in the χ_2^0 rest frame, which allows the kinematics to be reconstructed in the laboratory frame [17].

Oppositely-charged leptons are selected in a $\pm 15\,\mathrm{GeV}/c^2$ window around the end point of the mass distribution, and the χ_2^0 kinematics is reconstructed. The most energetic, b-tagged jet is then associated to the χ_2^0 to reconstruct the $\widetilde{\mathrm{b}} \to \mathrm{b}\chi_2^0$ decay. The resulting sbottom mass distribution for an integrated luminosity of $10\,\mathrm{fb}^{-1}$ is displayed in Fig. 12a.

Finally, the gluino decay to $\widetilde{\mathrm{b}}\overline{\mathrm{b}}$ is reconstructed by associating another b-tagged jet to the sbottom. The resulting gluino mass distribution with $10\,\mathrm{fb}^{-1}$ is shown in Fig. 12b.

The decay chain (b) can be reconstructed with a similar method, which requires the most energetic anti-b-tagged jet to be associated with the χ_2^0 instead of the most energetic b-tagged jet. Because the squark cross section is four times larger than the sbottom cross section (the supersymmetric partner of the u, d, s and c quarks are mass degenerate and all contribute democratically to the cross section), the common squark mass can be reconstructed with an integrated luminosity as small as $1\,\mathrm{fb}^{-1}$, and with a resolution similar to that obtained with $10\,\mathrm{fb}^{-1}$ for the sbottom.

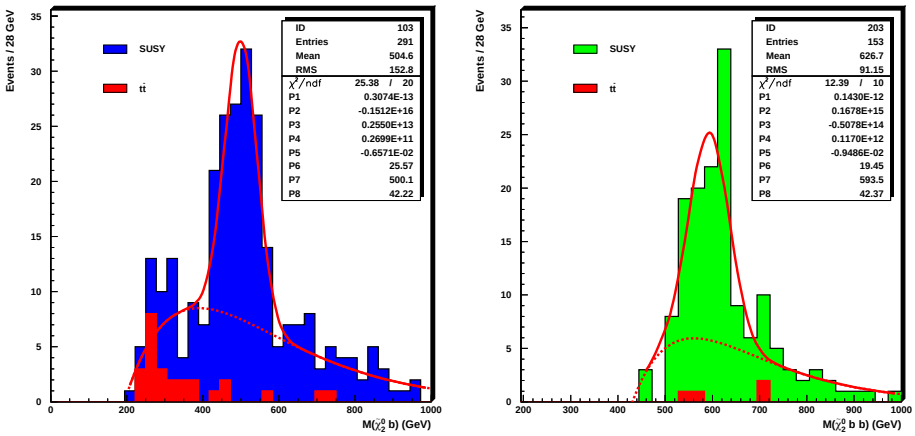

(a) Sbottom. (b) Gluino.

Fig. 12. Results from invariant mass fits for reconstructed sparticles with $10\,\mathrm{fb}^{-1}$ integrated luminosity at point B [15]. A Gaussian function is used for the signal peak, whereas the combinatorial and Standard Model backgrounds are fitted with a polynomial.

4 Conclusions and Outlook

At the start-up of the LHC, CMS will have in place a detector fulfilling the requirements for doing physics with an anticipated integrated luminosity of 5-10 fb^{-1} from the first physics run. Tracker, calorimeters, and muon barrel will be complete and will allow the reconstruction of leptons, missing energy and jets. Only items with a small impact on the low-luminosity performance will be staged and will be installed in time for the subsequent high-luminosity run.

Interesting physics is expected to appear immediately at the turn on provided the detector provides accurate charged particle momentum measurement, availability of vertexing information and full calorimetric coverage in pseudorapidity. The pixel system is a crucial component and as such it has to be commissioned very early to allow the online selection of electrons, photons and taus. A fast understanding of the alignment of the full silicon tracker will be mandatory to improve the online measurement of the muon transverse momenta and to apply lepton isolation criteria.

For an effective measurement of E_T^{miss} and jet energies the HCAL calibration has to be about 2%. For online electron and photon selection a calibration of ECAL to ~2% is sufficient. The ultimate goal for the search for the decay $\mathrm{H} \to \gamma\gamma$ is to reach offline an intercalibration of all crystals to 0.5%.

The full Standard Model Higgs boson mass range between 130 and 700 $\mathrm{GeV/c^2}$ will be covered with a few fb^{-1}, through fully leptonic decays as soon as an appropriate lepton identification efficiency is ensured. The lower part of the spectrum, between 115 and 130 $\mathrm{GeV/c^2}$, requires about 10 fb^{-1} and a fully aligned and calibrated detector. In the MSSM, additional Higgs physics states can be discovered as well in the $\mu\mu$ and $\tau\tau$ decay channels, through the associated production $\mathrm{gg} \to \mathrm{b\bar{b}}\ \mathrm{H/A}$, if $\tan\beta$ is large enough, with a couple of fb^{-1}. Finally, squarks and gluinos with masses up to 1.5 TeV/c^2 can be discovered with 1 fb^{-1} or less while their masses and decay chains can be reconstructed within favourable theoretical assumptions.

References

1. J.Virdee, Report from the Evian Meeting March 2003, *Requirements from Experiments in Year 1*
2. J.Rohlf: *Physics reach with CMS at high and super-high luminosities.* These proceedings
3. CERN/LHCC 2002-26, CMS TDR 6.2, 15 December 2002 *The Trigger and Data Aquisition project, Volume II, Data Aquisition & High-Level Trigger*
4. C.Seez: *The CMS trigger.* These proceedings
5. CERN/LHCC 97-32, CMS TDR 3, 15 December 1997 *The Muon Project*
6. D.Acosta, M.Stoutimore, S.M.Wang: CMS Note 2001/033 *Simulated Performance of the CSC Track-Finder*
7. CERN/LHCC 97-33, CMS TDR 4, 15 December 1997 *The Electromagnetic Calorimeter Project*
8. D.Futyan, C.Seez: CMS Note 2002/031. *Intercalibration of ECAL Crystals in Phi Using Symmetry of Energy Deposition*, To be published in J. Phys. A.

9. G.Dissertori: *Electromagnetic Calorimetry and* e/γ *Performance in CMS.* These proceedings
10. CERN/LHCC 97-31, CMS TDR 2, 20 June 1997 *The HCAL Project*
11. The HCAL group: in preparation for publication. *Performance and Calibration of CMS Hadron-Barrel Calorimeter Wedges*
12. CERN/LHCC 98-6, CMS TDR 5, 15 April 1998 *The Tracker Project*
13. R.Kinnunen et al: CMS Note in preparation, *Summary of the CMS Discovery Potential for the Higgs boson(s)*
14. S.Lehti, CMS Note 2002/035, *Study of* $gg \to b\bar{b}H_{SUSY}, H_{SUSY} \to \tau\tau \to \ell\ell + X$
15. M.Chiorboli: PhD Thesis, *Supersymmetric Particle Reconstruction with the CMS Detector at the LHC*, Universita degli studi di Catania.
16. M.Battaglia et al: *Proposed Post-LEP Benchmarks for Supersymmetry*, Eur.Phys.J. C22 (2001) 535
17. H.Baer, C.H.Chen, F.Paige, X.Tata, Phys.Rev.D50 (1994) 4508. I.Iashvili, A.Kharchilava: CMS Note 1997-065 D.Denegri, W.Majerotto, L.Rurua, Phys.Rev.D 60, 035008 (1999), CMS Note 1998-085